Nonlinear Processes
in Geophysics

An upper limit for slow-earthquake zones: self-oscillatory behavior through the Hopf bifurcation mechanism from a spring-block model under lubricated surfaces

Valentina Castellanos-Rodríguez[1,2], **Eric Campos-Cantón**[2,3], **Rafael Barboza-Gudiño**[1], **and Ricardo Femat**[2]

[1]Instituto de Geología, Universidad Autónoma de San Luis Potosí, San Luis Potosí, México
[2]Instituto Potosino de Investigación Científica y Tecnológica A.C., San Luis Potosí, México
[3]Mathematics Department, University of Houston, Houston, Texas 77204-3008, USA

Correspondence to: Castellanos-Rodríguez Valentina (valentina@cimat.mx)

Abstract. The complex oscillatory behavior of a spring-block model is analyzed via the Hopf bifurcation mechanism. The mathematical spring-block model includes Dieterich–Ruina's friction law and Stribeck's effect. The existence of self-sustained oscillations in the transition zone – where slow earthquakes are generated within the frictionally unstable region – is determined. An upper limit for this region is proposed as a function of seismic parameters and frictional coefficients which are concerned with presence of fluids in the system. The importance of the characteristic length scale L, the implications of fluids, and the effects of external perturbations in the complex dynamic oscillatory behavior, as well as in the stationary solution, are take into consideration.

1   Introduction

In the last decade, the study of slow earthquakes (tremors, low and very low frequencies events, and slow slip events) has become of great relevance because of its possible relationship with the occurrence of large earthquakes. The stress redistribution of slow earthquakes, and the strain in the lowest limit of the seismogenic layer caused by them, could be helpful for a better understanding of the nucleation process of ordinary earthquakes (Ide et al., 2007; Wech and Creager, 2007; Beroza and Ide, 2009; Peng and Gomberg, 2010; Rivet et al., 2011; Ikari et al., 2013; Jolivet et al., 2013; Abe and Kato, 2014; Audet and Bürgmann, 2011; Bürgmann, 2014; Wallace et al., 2016). Although most slow earthquakes have

been detected in subduction zones, there are reports of these in other types of faults (Vergnolle et al., 2010; Thomas et al., 2016; Wallace et al., 2016).

Observations suggest that this occurs between the seismogenic zone and the frictionally stable zone (Fig. 1) surrounding the critical value of ordinary-earthquake nucleation; i.e., on parts of faults where the behavior is transitional between frictional properties on the rocks and slow, steady deformation (Scholz, 1998; Dragert et al., 2001; Beroza and Ide, 2009; Abe and Kato, 2014; Watkins et al., 2015), but some investigation revealed that slow earthquakes have been observed in shallow regions (Davis et al., 2011; Nishimura, 2014; Saffer and Wallace, 2015; Valée et al., 2015; Yamashita et al., 2015; Wallace et al., 2016). Figure 1 shows two stability regions and transition zones: at shallow depth and on the base of the seismogenic layer (Scholz, 1998), the latter of which is the focus of the study presented in this paper.

Scholz (1998) determined that at the border of the stability transition there is a region in which self-sustained oscillatory motion occurs into the conditionally stable region, below the critical point, where slow earthquakes are nucleated. These oscillations are observed in the presence or absence of external forces such as vibrations from neighbor faults but eventually tend to stabilize.

Slow earthquakes occur in a variety of stick slip (Ide et al., 2007). Watkins et al. (2015) say that observational studies have provided information for their characterization (variability in duration, recurrence, and propagation velocity), but the mechanism of slow earthquakes is still unclear. Experi-
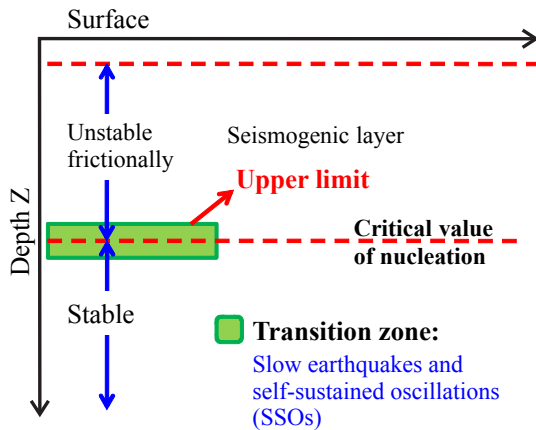
Figure 1. Transition zone related to slow-earthquake nucleation. The first dashed red line indicates the lowest limit of the shallow frictionally stable region. The second one shows the deeper limit of the seismogenic layer (upper limit of the deeper frictionally stable region). Self-oscillatory behavior is observed in the second transition.

mental data show that the physical and mechanical parameters that control changes in slow slip events are the rates of convergence, frictional parameters and effective normal stress, under rate- and state-dependent constitutive properties of Dieterich–Ruina friction law (Dieterich, 1979; Ruina, 1983; Watkins et al., 2015; Marone et al., 2015; Scuderi et al., 2016).

The Dieterich–Ruina friction law has been successfully used to reproduce the stick-slip behavior in the models of earthquakes dynamics and slow earthquakes. Spring-block models have reproduced these events when coupled with rate- and state-dependent friction laws, and by contrast, models which have been used with laws velocity-weakening friction and constant friction have not been successful (Abe and Kato, 2014). Beroza and Ide (2009) infer that simple friction laws by themselves do not provide an explanation for the complex behavior of slow earthquakes. Some investigations have suggested that fluids play an important role in this mechanism (Brown et al., 2005; Ide et al., 2007; Wallace et al., 2016). Some studies support this idea: conclusions from revised literature establish that failures are lubricated on the shear area regardless of the composition of the rocks and the frictional weakening mechanism involved (Faulkner et al., 2010; Di Toro et al., 2011).

An important issue of the rate- and state-dependent friction law is that it is totally macroscopic, i.e., it describes the frictional properties of the system rather than the microscopic mechanism which is responsible for the dissipation (Ruina, 1983; Carlson and Batista, 1996; Batista and Carlson, 1998). Experimental research on the role of fluids in the ordinary-earthquake mechanisms has captured specific features associated with the molecular-layer lubrication on the border between two surfaces in contact, with different fric-

tional properties when considering lubricants in volume and dry interfaces (Gee et al., 1990; Yoshizawa and Israelachvili, 1993; Reiter et al., 1994; Carlson and Batista, 1996; Batista and Carlson, 1998; Amendola and Dragoni, 2013). The initiation slip on the microscopic scale is associated with a shear melting transition in the lubricant layer (Carlson and Batista, 1996) so that microscopic scales contribute to better understanding of the friction mechanism.

A path to study slow earthquakes is through the spring-block model for ordinary earthquakes, because both the slow and ordinary earthquakes are related by the critical value of nucleation. Some spring-block models display complex oscillatory behavior associated with the transition zone (Gu et al., 1984; Abe and Kato, 2013, 2014).

Gu et al. (1984) and Abe and Kato (2013), used a spring-block model where complex oscillatory behavior was found near to a critical value of the earthquakes nucleation. This behavior is presented as changing when there is a variation in any parameter related to the critical value.

Batista and Carlson (1998) introduced, in a spring-block model, an alternative friction law, where the state variable is interpreted in terms of the shear melting of the lubricant (molecular layer of lubricant) between solid surfaces in contact. They considered that by incorporating the microscopic mechanism it could determine other behavior and found that the transition from steady sliding to stick slip is typically discontinuous and sometimes hysteretic. This transition is associated with a subcritical Hopf bifurcation (set of seismic parameters for the critical point of nucleation). Gu et al. (1984), Abe and Kato (2013), and Batista and Carlson (1998) observed a sudden and discontinuous onset in the amplitude of oscillations at the bifurcation point. Surrounding the transition, complex oscillatory behavior was observed in these cases.

In terms of dynamical systems based on the spring-block model, the presence of oscillations and self-oscillations can be explained by the Hopf bifurcation mechanism (Kengne et al., 2014; Meng and Huo, 2014; Wang et al., 2014). Some nonlinear dynamical systems show self-sustained oscillation (SSO) motion (Strogatz, 1994), one of them being relative to the earthquake physics mechanism (Scholz, 1998). The SSO behavior would be explained in the context of the complex system of faults, such that the modeling of movement in a single failure would be affected by external forces (Chelidze et al., 2005). These forces can be generated due to vibrations or stress transferred from neighboring faults, that make the system go from a limit cycle to another, leaving different paths of recurrence (Chelidze et al., 2005; Dragoni and Santini, 2010; Dragoni and Piombo, 2011).

In this paper the main objective is to propose an upper limit for the SSO region in the frictionally unstable zone (Fig. 1). The upper limit is a function of mathematical and numerical relations in terms of seismic and frictional parameters. This limit describes the complexity of the oscillatory movement in
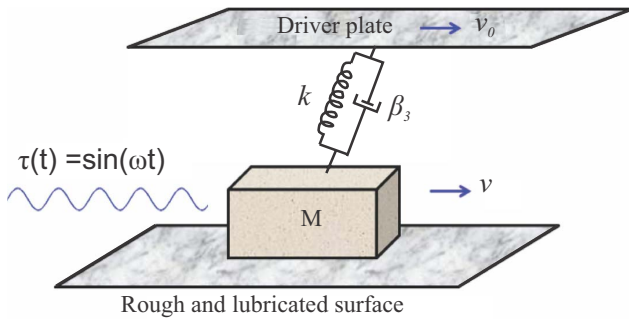
Figure 2. Dieterich–Ruina–Stribeck one-degree-of-freedom oscillator. Here, v_0 is a reference velocity, v is the block velocity, k is the constant of deformation, and β_3 is the dynamical viscosity coefficient; $\tau(t)$ is an external and perturbing force with angular frequency ω.

the nearest region to the critical point of nucleation. Another objective is to determine the role of the fluids in this region.

The oscillatory behavior of the system is studied through analysis of the Madariaga spring-block model (Erickson et al., 2008) complemented by the Stribeck effect (Alvarez-Ramírez et al., 1995; Andersson et al., 2007). The Stribeck effect shows the transition from dry interfaces or lubricated at the border until separated by a layer of lubricant as a shear melting. This effect takes into account the microscopic mechanism between the contacting surfaces during displacement. The Dieterich–Ruina–Stribeck (DR-S) oscillator (Fig. 2) depicts the behavior of the kinetic mechanism between tectonic blocks in the Earth's crust undergoing stick-slip effects from friction. The oscillator is coupled to a driven plate by the rheological properties of rocks, and to a static plate by frictional properties. The slider is on the rough and lubricated surface. The relative displacement, rate of displacement, and acceleration are given by $u = y - v_0 t$, $\dot{u} = v - v_0$, and $\ddot{u} = \dot{v}$, respectively, where y is the block displacement and $v = \dot{y}$.

An external periodic perturbation $\tau(t)$ is introduced in order to show that this system exhibits SSO behavior between the critical point of nucleation and the region limited by the proposed upper limit. In Sect. 2 the model is proposed, and the linearized system, stationary solution, and criterion for frictional stability are analyzed. In Sect. 3 the oscillatory behavior is described, the upper limit of SSO region is proposed, and numerical simulations are provided. Finally, in Sect. 4 a brief discussion of the outcomes and conclusions are presented.

2 Nonlinear dynamical system

2.1 The model

The faults are lubricated in the shear area (Faulkner et al., 2010; Di Toro et al., 2011) as the most sliding contacts. A model based in a slider block (Fig. 2) is essen-

tially a mechanic representation, and the frictional components are velocity-dependent. Andersson et al. (2007) explain Stribeck's effect as follows. The friction force varies with the sliding speed depending on the extent to which the interacting contact surfaces are running under boundary, mixed (fluid in the union between asperities), or full film lubrication (a layer of fluid as a shear melting). Even dry contacts show some behavior similar to that in lubricated contacts in that they have a higher static friction than dynamic or sliding friction. In lubricated sliding contacts, the friction decreases with increasing sliding speed until a mixed or full film situation is obtained, after which the friction in the contact can be constant, increasing or decreasing somewhat with increasing sliding speed due to viscous and thermal effects. This transition is named Stribeck's effect (Jacobson, 2003; Andersson et al., 2007) and has been formulated as follows:

$$F_s(v) = \beta_1 \text{sign}(v - v_0) + \beta_2 e^{-\mu(v)}\text{sign}(v - v_0) + \beta_3 v, \quad (1)$$

where β_1 is the Coulomb friction, $\beta_2 = F_{\max} - \beta_1$ (with $F_{\max}$ as the upper limit of static force), β_3 represents the dynamical viscosity coefficient of the fluid, and μ denotes a slip constant or decay parameter for the mixed lubrication.

On the other hand, the well known phenomenological friction law of Dieterich–Ruina is introduced in rock mechanics to capture experimental observations of steady state and transient friction that depends on the displacement history effects (state variable θ) and velocity (Dieterich, 1979; Ruina, 1983; Dieterich and Kilgore, 1994), one of its formulations is given by two equations (Ruina, 1983):

$$F_{\mathrm{dr}}(v, \theta) = \theta + A \ln(v/v_0),$$
$$\dot{\theta} = -(v/L)\left[\theta + B \ln(v/v_0)\right]. \quad (2)$$

The first equation represents the frictional stress under a stable state ($\dot{\theta} = 0$), and the second one corresponds to evolution of state variable θ that evolves with time, slip, and normal stress history (Dieterich and Kilgore, 1994). L is a characteristic sliding distance over which θ evolves (required distance to renew the contact population). A and B are material properties, and we assume $B > A > 0$ for frictional instability.

Now it is possible to derive from Eqs. (1) and (2) an alternative friction law taking into account the macroscopic and microscopic mechanism (frictional properties and dissipation). The equation of motion derived from Eqs. (1) and (2) gives a first-order differential equation system; a similar expression is given by Erickson et al. (2008), but we complemented their system by the term of Stribeck's effect:

$$\dot{\theta} = -(v/L)[\theta + B \ln(v/v_0)],$$
$$\dot{u} = v - v_0,$$
$$\dot{v} = -(1/M)[ku + F_{\mathrm{dr}}(v, \theta)]$$
$$\quad - (1/M)F_0(v) + \tau(t), \quad (3)$$

where Stribeck's effect from Eq. (1) is given now by

$$F_0(v) = \beta_1 + \beta_2 e^{-\mu(v)} + \beta_3 v. \quad (4)$$

Note that the slider block velocity is relative to velocity of driver plate. From the second equation of the system Eq. (3), we infer that the block will oscillate with respect to the position of the plate. This equation tells us whether the oscillator is to the right or to the left with respect to the driver plate. Although the direction of the displacement of the system is always forward if $v - v_0 > 0$, i.e., if $v > v_0$, eventually the oscillator will be more advanced than the plate. Conversely, if $v - v_0 < 0$, i.e., $v < v_0$ eventually the oscillator will be to the left of the plate. One of the objectives when introducing the function $\text{sign}(v - v_0)$ in the Eq. (1) is to indicate this effect; assigning value 1 for the first case, -1 for the second case, and zero otherwise. We eliminate the sign function because this effect is already considered in the second equation of the system Eq. (3).

Defining new variables $\hat{\theta}, \hat{v}, \hat{u}$, and $\hat{t}$ (Erickson et al., 2008) as $\theta/A = \hat{\theta}, v/v_0 = \hat{v}, u/L = \hat{u}, t(v_0/L) = \hat{t}$, the dimensionless system is given by the following equations:

$$\dot{\hat{\theta}} = -\hat{v}[\hat{\theta} + (1 + \varepsilon)\ln(\hat{v})],$$
$$\dot{\hat{u}} = \hat{v} - 1,$$
$$\dot{\hat{v}} = -\gamma^2[\hat{u} + (1/\xi)(\hat{\theta} + \ln(\hat{v}))] - \alpha F_0(\hat{v}) + \hat{\tau}(\hat{t}), \quad (5)$$

where $\boldsymbol{\alpha} = (\alpha_1, \alpha_2, \alpha_3)$; $\alpha_{1,2} = \frac{L\beta_2}{v_0^2 M}$, $\alpha_3 = \frac{L\beta_3}{v_0 M}$. The external force is $\hat{\tau}(\hat{t}) = \hat{c}\sin(\hat{w}\hat{t})$, where $\hat{c} = \frac{L}{v_0^2}$ and $\hat{w} = \frac{Lw}{v_0}$. The frictional parameters $\boldsymbol{\alpha}$ are associated with frictional coefficients from the Stribeck effect and

$$\alpha F_0(\hat{v}) = \alpha_1 + \alpha_2 e^{-\hat{\mu}\hat{v}} + \alpha_3 \hat{v}, \qquad \hat{\mu} = v_0 \mu. \quad (6)$$

The variable $\boldsymbol{x} = (\hat{\theta}, \hat{u}, \hat{v})$ is the dimensionless state variable, and $\hat{\theta}$ stands for the measurement of contact with asperities from the Dieterich–Ruina friction law; $\hat{u}$ is the dimensionless relative displacement between the block and the upper plate, and $\hat{v} > 0$ is the dimensionless velocity of the block. The function $\boldsymbol{f}(\boldsymbol{x})$ on the right-hand side of Eq. (5) defines a mapping $\boldsymbol{f}: \mathbb{R}^3 \rightarrow \mathbb{R}^3$. This mapping defines a vector field on $\mathbb{R}^3$. Thus, the system given by Eq. (5) induces in phase space $\mathbb{R}^3$ the flow $(\boldsymbol{\varphi}^t)$, and $t \in \mathbb{R}$ such that each forward trajectory of the initial point $\boldsymbol{x}_0 = \boldsymbol{x}(t = 0)$ is the set $\{\boldsymbol{x}(t) = \boldsymbol{\varphi}^t(\boldsymbol{x}_0) : t \geq 0\}$.

Parameters $\boldsymbol{\Pi} = (\varepsilon, \xi, \gamma)$ are given as follows: $\varepsilon = (B - A)/A$, $\xi = kL/A$, and $\gamma = \sqrt{(k/M)}(L/v_0)$, associated with stress drop during displacement, deformation, and the oscillation frequency, respectively. The Eq. (5) is referred to the system of DR-S where $\hat{\tau}(\hat{t})$ is the periodical and deterministic external force $\hat{\tau}(\hat{t}) = \hat{c}\sin(\hat{\omega}\hat{t})$; here $\hat{\omega}$ is the angular frequency. We designated a system as an unperturbed system when $\hat{\tau}(\hat{t}) = 0$ and a perturbed system otherwise. We will denote $(\hat{\theta}, \hat{u}, \hat{v}) := (\theta, u, v)$, $\hat{\tau}(\hat{t}) := \tau(t)$, $\hat{\omega} := \omega$, $\hat{c} := c$, and $\hat{\mu} := \mu$.

2.2 Stationary solution at equilibrium point

The stationary solution $\boldsymbol{x} = \boldsymbol{x}^*$ of the system Eq. (5) with $\tau(t) = 0$ is given by

$$\boldsymbol{x}^* = (\theta^*, u^*, v^*) = (0, \eta, 1),$$
$$u^* = \eta = (\alpha_1 + \alpha_2 e^{-\mu} + \alpha_3)/\gamma^2, \gamma > 0, \quad (7)$$

where η corresponds to the relative position of the single slider block. At $\boldsymbol{x}^*$ the plate and the block have the same velocity and the measure of the asperities contact is zero. Note that θ^* and v^* do not depend on $\boldsymbol{\Pi}$ but u^* depends on frequency oscillation γ (consequently on kL) and frictional constants of Stribeck's effect, both are associated with the energy dissipation.

In the spring-block model, the logarithmic term in the Dieterich–Ruina friction law has introduced greater difficulties in solving the problem. Due to the nonlinear term, analytic integration has not been possible, and even numerical solutions present challenges because of the logarithmic term (Erickson et al., 2008). The linearized system analysis is very useful to describe some features of the nonlinear system about a steady-state solution (Gu et al., 1984; Shkoller and Minster, 1997; Erickson et al., 2008). The local and asymptotic stability of $\boldsymbol{x}^*$ is analyzed with the indirect method of Lyapunov that consists of the analysis of the eigenvalues of the Jacobian matrix from the linearized system of Eq. (5) around the stationary solution (Khalil, 1996). Let $\boldsymbol{x}^*$ be locally asymptotically stable, i. e., every solution of the system $\boldsymbol{\varphi}^t(\boldsymbol{x}_0) = (\theta(t), u(t), v(t))$; starting near to the stationary solution, it remains at the surrounding of $\boldsymbol{x}^*$ all the time, and eventually the solution converges to $\boldsymbol{x}^*$ (convergence to frictional stability). Let us denote the Jacobian matrix as $\mathrm{D}_f(\boldsymbol{x}^*) = (\partial f_i(x)/\partial x_j)|_{\boldsymbol{x}^*}$, for $i, j = 1, 2, 3$, where $\boldsymbol{f}(\boldsymbol{x}) = (f_1, f_2, f_3)$ is the vector field given by the right-hand side of Eq. (5), with $\tau(t) = 0$, $(x_1, x_2, x_3) = (\theta, u, v)$, and λ_i be the eigenvalues of $\mathrm{D}_f(\boldsymbol{x}^*)$:

$$\mathrm{D}_f(\boldsymbol{x}^*) = \begin{pmatrix} -1 & 0 & -(1+\varepsilon) \\ 0 & 0 & 1 \\ -\gamma^2/\xi & -\gamma^2 & -\gamma^2/\xi - \phi \end{pmatrix}, \quad (8)$$

where $\phi = \alpha_2 \mu e^{-\mu} - \alpha_3$. The characteristic polynomial of Eq. (8) is given by the following:

$$P(\lambda) = a_0 \lambda^3 + a_1 \lambda^2 + a_2 \lambda + a_3, \quad (9)$$

whose coefficients are in terms of seismic parameters $\boldsymbol{\Pi}$ and frictional coefficients $\boldsymbol{\alpha}$ and μ.

$$a_0 = 1$$
$$a_1 = 1 + \gamma^2/\xi + \phi$$
$$a_2 = \gamma^2(1 - \varepsilon/\xi) + \phi$$
$$a_3 = \gamma^2 \quad (10)$$

The dynamical system of earthquakes is a naturally dissipative phenomenon, and due to this feature the dissipativ-

ity condition of the stationary solution is required. Thus, locally the system is dissipative at $\boldsymbol{x}^*$ if $a_1 = -\operatorname{Trace} \mathrm{D}_f(\boldsymbol{x}^*) = \sum_{i=1}^{3} \lambda_i < 0$ that is true under the following condition:

$$\frac{Mv_0}{L} + \frac{A}{v_0} + \beta_2 \mu e^{-\mu v_0} < \beta_3. \tag{11}$$

Equation (11) comes directly from $a_1 < 0$ and the values of γ, ε, ξ, and ϕ. The Eq. (11) is the necessary condition for the system to be subdamped , and oscillations can be observed; moreover, due to $a_3 = -\det \mathrm{D}_f(\boldsymbol{x}^*) < 0$, $\boldsymbol{x}^*$ is hyperbolic. Through the analysis of the eigenvalues of $\mathrm{D}_f(\boldsymbol{x}^*)$ we will explain what implies a hyperbolic equilibrium point related to oscillatory behavior.

3 Oscillatory behavior

Earthquake dynamics are a nonlinear oscillatory phenomenon (Gu et al., 1984; De Sousa Vieira, 1995; Levin, 1996; Chelidze et al., 2005; Maloney and Robbins, 2007; Erickson et al., 2008; Dragoni and Santini, 2010; Castellanos-Rodríguez and Femat, 2013; Amendola and Dragoni, 2013; Abe and Kato, 2014), where the nonlinear complex behavior is attributable to the friction forces. The analysis of the oscillatory behavior is explored in this section. We use the full nonlinear term in the numerical simulation in Sect. 3.2 and 3.3.

3.1 Analysis of eigenvalues

The equilibrium point $\boldsymbol{x}^*$ is locally asymptotically stable if the real part of all the eigenvalues is negative, i.e., $Re(\lambda_i) < 0$, and it is unstable if at least one eigenvalue of $\mathrm{D}_f(\boldsymbol{x}^*)$ is positive, i.e., $Re(\lambda_i) \geq 0$. We are interested in the type of hyperbolic stationary solution $\boldsymbol{x}^* = (0, \eta, 1)$: it has a stable manifold, i.e., $Re\{\lambda_i\} < 0$, $Im\{\lambda_i\} = 0$, and a unstable manifold that generates oscillations in a plane, i.e., $Re\{\lambda_k\} > 0$, $Im\{\lambda_k\} \neq 0$ (Campos-Cantón et al., 2010).

A sufficient condition for local and asymptotic stability comes from the Routh–Hurwitz criterion, i.e., the sufficient conditions to ensure that Jacobian matrix Eq. (8) has three eigenvalues with a negative real part are that the coefficients of the characteristic polynomial holds the following inequalities:

$$a_0, a_1, a_2, a_3 > 0, \qquad a_1 a_2 - a_0 a_3 > 0. \tag{12}$$

Note that the first inequality holds ($a_0, a_3 > 0$), and $a_1 > 0$ because $\phi < 1$ and $\boldsymbol{\Pi} > 0$; if $\operatorname{sign}(a_2) > 0$ we deduce that

$$\varepsilon < \xi\psi \quad \text{and} \qquad \psi = 1 + \phi/\gamma^2 \tag{13}$$

as necessary conditions for stability but are not sufficient. The sufficient condition for stability comes from the second inequality of Eq. (12) and $a_2 > 0$ as follows:

$$\varepsilon < \xi\left[1 - \frac{1}{1 + \gamma^2/\xi + \phi} + \frac{\phi}{\gamma^2}\right]. \tag{14}$$

For the region with the sufficient condition Eq. (14), all eigenvalues of the Jacobian matrix Eq. (8) have negative real part and the equilibrium point $\boldsymbol{x}^* = (0, \eta, 1)$ is a sink (Perko et al., 2001).

The relationship between the parameters $\boldsymbol{\Pi}$ associated with the necessary condition Eq. (13) and sufficient condition Eq. (14) are described in Fig. 3a, b, and c, for fixed $\xi = 0.4, 0.8, 1$, respectively. By means of numerical simulation the stability was computed and found for values of $\gamma > 0.5$.

In order to determine how many eigenvalues of $\mathrm{D}_f(\boldsymbol{x}^*)$ are real or complex conjugates, Descartes' rule of signs to analyze the roots of the characteristic polynomial is used. Under the condition Eq. (11), signs of coefficients Eq. (10) are

$$(+, +, \operatorname{sign}(a_2), +). \tag{15}$$

If $\operatorname{sign}(a_2) > 0$ there are two possibilities: all eigenvalues are negative real, i. e., $Re\{\lambda_i\} < 0$, $Im\{\lambda_i\} = 0$, or one eigenvalue is negative real and the other two are complex conjugates; the last statement corresponds to the oscillatory behavior.

On the other hand, if $\operatorname{sign}(a_2) < 0$, there are possibly two positive real eigenvalues, i.e., $Re\{\lambda_k\} > 0$, $Im\{\lambda_k\} = 0$ and one negative real; for this case there are no complex conjugate eigenvalues, and hence nonoscillatory behavior is observed. For all cases there is one negative real eigenvalue, the other two could be complex conjugates or positive real. Figure 4 shows the locus of the real part of two eigenvalues corresponding to the oscillatory and the nonoscillatory behavior; it describes the relationship between parameters $\boldsymbol{\Pi}$. The graph for the negative real eigenvalue was omitted because we focused on complex eigenvalues.

The oscillatory behavior is located before the branching, after which the system ceases to oscillate. The locus of the eigenvalues for different values of $\xi = 0.4, 0.8, 1$ are shown in Fig. 4a, b for $\gamma = 0.8$ and $\gamma = 10$, respectively. The range of ε decreases with the increasing of γ and the decreasing of ξ. Figure 4c and d describe the same behavior as explained above, and it was observed that for values of $\gamma > 10$ the range of ε for oscillatory behavior is almost equal, although after the branching point with the increasing of γ, one of the eigenvalues increases rapidly (i.e., kL increases, making the system stiffness the biggest or making L increase) and the other one tends to zero, more quickly.

A set of parameters was found that satisfies the necessary condition Eq. (13) for stability, within an unstable and oscillatory region which is around the Hopf bifurcation (set of seismic parameters that satisfies the critical value of nucleation; Fig. 1). The region with these features is proposed for the region of self-sustained oscillations and consequently for the slow-earthquake zone. The SSO region is in the unstable region and will be explored in the follow sections.
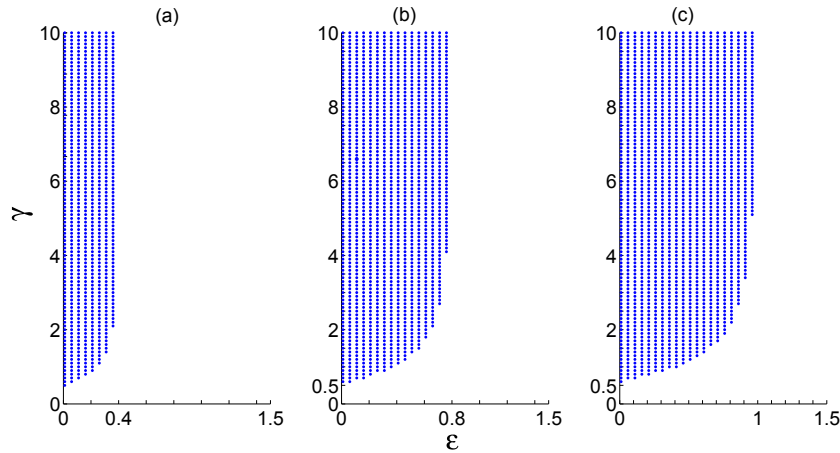
Figure 3. Stability region for homogeneous system ($\tau(t) = 0$), as a function of (ε, ξ, γ) for fixed values of ξ. **(a)** $\xi = 0.4$, **(b)** $\xi = 0.8$, and **(c)** $\xi = 1$. The necessary and sufficient conditions are satisfied.
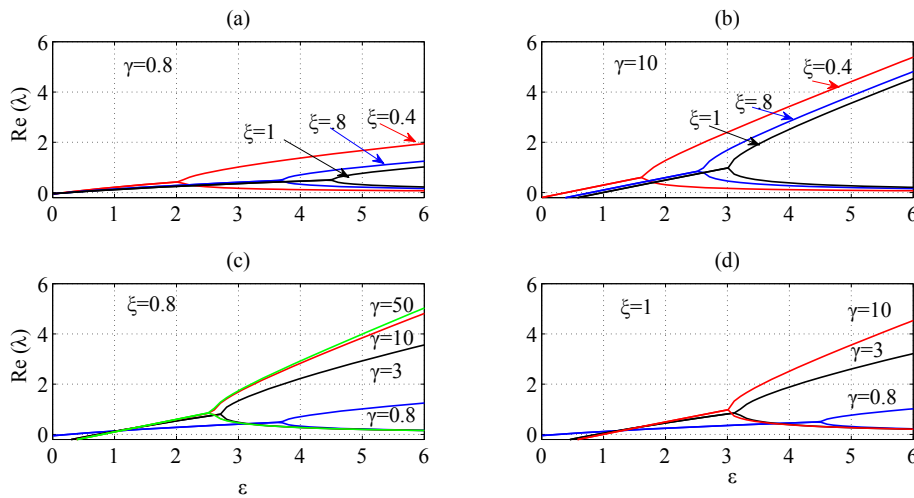

Figure 4. Loci of eigenvalues for different values of ξ and γ. The Figure shows the real part of eigenvalues as a function of parameters ε, ξ and γ. For **(a)** and **(b)** fixed $\gamma = 0.8$ and 10, respectively; **(c)** and **(d)** shows eigenvalues for fixed $\xi = 0.8$ and 1, respectively.

3.2 A Hopf bifurcation, oscillatory range (OR) and the self-sustained oscillation (SSO) region

The presence of oscillations in physical systems can be explained through the mechanism of Hopf bifurcation. When three eigenvalues exist, and two of them are complex conjugates and the other is a nonzero real, a Hopf bifurcation occurs (Fig. 5) if the real part of the complex eigenvalues cross the imaginary axis. Periodic orbits and limit cycles are either created or destroyed for the nearest values of the Hopf bifurcation (Guckenheimer and Holmes, 1983). If all neighboring trajectories approach the limit cycle then it can be said that the limit cycle is stable or an attractor. Stable limit cycles are important because they model systems that exhibit SSO behavior (Strogatz, 1994), therefore starting at Hopf bifurcation, the oscillatory behavior around it will be analyzed.

There are three necessary conditions in order for a Hopf bifurcation to occur: (i) The existence of an equilibrium point, $f(x^*) = 0$; (ii) the Jacobian matrix $D_f(x^*)$ has a couple of eigenvalues on the imaginary axis, i. e., $Re\{\lambda_{1,2}\} = 0$ and $Im\{\lambda_{1,2}\} \neq 0$; and (iii) the cross-velocity of eigenvalues through imaginary axis must be different to zero.

For any system with three variables, the conditions (ii) and (iii) for obtaining a Hopf bifurcation are given in terms of the characteristic polynomial coefficients a_1, a_2, and a_3 from Eq. (10) (Baca, 2007). The cross velocity is given by the derivative $r'(\mathbf{\Pi}_0) = \frac{d}{d\gamma}(Re\{\lambda(\mathbf{\Pi})\})|_{\gamma=\gamma_0} \neq 0$, where $\mathbf{\Pi}_0 = (\varepsilon_0, \xi_0, \gamma_0)$ is a set of fixed values and $\lambda(\mathbf{\Pi})$ is an eigenvalue of $D_f(x^*)$ at $\mathbf{\Pi}$. The derivative is with respect to the bifurcation parameter, γ (oscillation frequency). The cross velocity
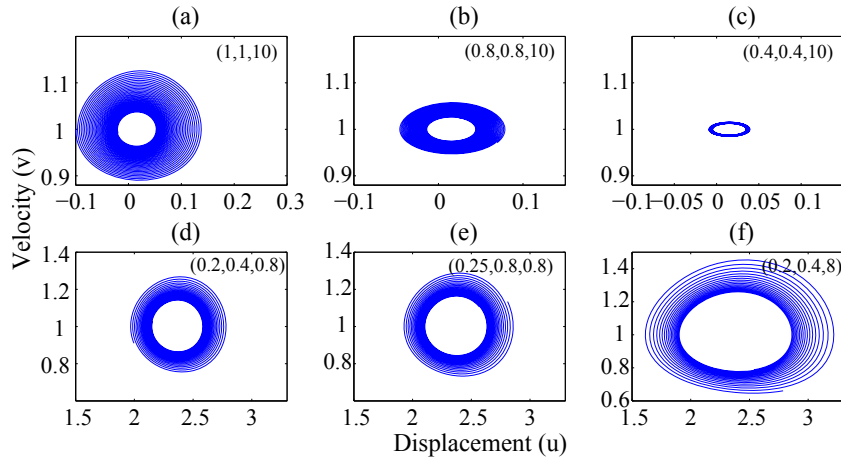
Figure 5. Unperturbed system $\tau(t) = 0$. Projection of attractor onto the plane (u, v). Panels **(a)**, **(b)**, and **(c)** have the position of equilibrium point $u^* = \eta$ near zero for $\gamma = 10$, and ξ decreases as it is the range of u. Panels **(d)**, **(e)**, and **(f)**, for $\gamma = 0.8$, have both u^* and the range of values for u higher than **(a)**–**(c)**.

is

$$r'(\mathbf{\Pi}_0) = \frac{a_3'(\mathbf{\Pi}_0) - b^2 a_1'(\mathbf{\Pi}_0) + \lambda_0 a_2'(\mathbf{\Pi}_0)}{2(\lambda_0^2 + b^2)},$$

$$a_1(\mathbf{\Pi}_0) = -\lambda_0,$$

and $a_2(\mathbf{\Pi}_0) = b^2$. $\qquad\qquad\qquad\qquad (16)$

The polynomial from Eq. (9) has a couple of imaginary roots $\lambda_{1,2}$ if there is a $\mathbf{\Pi}$ such that the following two relations are satisfied:

$$a_3 = a_1 a_2, \qquad a_2 > 0. \qquad\qquad\qquad (17)$$

If $\mathbf{\Pi} = \mathbf{\Pi}_0$ satisfies the Eq. (17), then the complex roots of Eq. (9) with real part zero are determined by

$$\lambda_{1,2} = \pm i b_0, \qquad b_0 = \sqrt{a_2}, \qquad \lambda_3 = -\frac{a_3}{a_2}. \qquad (18)$$

From Eqs. (10) and (18), the eigenvalues of Eq. (8) for the Hopf bifurcation are given by

$$\lambda_{1,2}(\mathbf{\Pi}_0) = \pm i \sqrt{\gamma_0^2 - \frac{\gamma_0^2 \varepsilon_{\mathrm{HB}}}{\xi_0} + \phi},$$

$$\lambda_3(\mathbf{\Pi}_0) = -\frac{\gamma_0^2}{\gamma_0^2 - \frac{\gamma_0^2 \varepsilon_{\mathrm{HB}}}{\xi_0} + \phi}. \qquad (19)$$

The Jacobian matrix Eq. (8) has two complex conjugate eigenvalues with a positive real part for values of ε which depend on the fixed values γ_0 and ξ_0. These eigenvalues correspond to oscillatory regions in the unstable regime, and they are observed from the Hopf bifurcation to the beginning of bifurcation as it is depicted in the Fig. 4; this interval is called the oscillatory range OR. We want to find the limits of OR and the SSO in terms of seismic parameters.

From Eqs. (10) and (17) it is determined $\varepsilon_{\mathrm{HB}}$, i.e., the ε value for the Hopf bifurcation

$$\varepsilon_{\mathrm{HB}} = \xi_0 \left[1 - \frac{1}{1 + \frac{\gamma_0^2}{\xi_0} + \phi} + \frac{\phi}{\gamma_0^2} \right], \qquad (20)$$

where $\varepsilon_{\mathrm{HB}}$ is the lower limit of OR. The upper limit is determined by the discriminant of the third-order polynomial $a_0 \lambda^3 + a_1 \lambda^2 + a_2 \lambda + a_3$:

$$D = \left(\frac{3a_2 - a_1^2}{9} \right)^3 + \left(\frac{9a_1 a_2 - 27 a_3 - 2a_1^3}{54} \right)^2. \qquad (21)$$

If $D > 0$ there are two complex conjugate roots and one is real; if $D = 0$ all are real roots, and at least two are equal; and if $D < 0$ all roots are real and unequal. We are interested in $D = 0$, which implies that the oscillatory behavior finishes (there are not complex roots). From Eqs. (9), (10), and (21)

$$D = \left[\frac{3\left(\gamma_0^2 - \frac{\gamma_0^2 \varepsilon_{D=0}}{\xi_0} + \phi\right) - \left(1 + \frac{\gamma_0^2}{\xi_0} + \phi\right)^2}{9} \right]^3 +$$

$$\left[\frac{9\left(1 + \frac{\gamma_0^2}{\xi_0} + \phi\right)\left(\gamma_0^2 - \frac{\gamma_0^2 \varepsilon_{D=0}}{\xi_0} + \phi\right) - 27\gamma_0^2 - 2\left(1 + \frac{\gamma_0^2}{\xi_0} + \phi\right)^3}{54} \right]^2 = 0,$$

and we can resolve by $\varepsilon_{D=0}$, according to Fig. 4. The OR for ε is in the interval

$$\mathrm{OR} \in (\varepsilon_{\mathrm{HB}}, \varepsilon_{D=0}). \qquad (22)$$

In the OR, the necessary condition Eq. (13) for stability is satisfied by a set of parameters $\mathbf{\Pi}$ around the Hopf bifurcation; the region with these features is proposed for the SSO.

The proposed interval for SSO is

$$\text{SSO} \in (\varepsilon_{\text{HB}}, \xi_0 \psi_0), \qquad \psi_0 = 1 + \frac{\phi}{\gamma_0^2}. \tag{23}$$

Some numerical results are summarized in Table 1.

Our interest is for the case that $\varepsilon = (B - A)/A > 0$, or $B - A > 0$, which means that the stress drop is negative and consequently an unstable regime is observed; under this assumption, $\xi \psi$ it is a positive amount implying that $\psi > 0$. Equation (13) is a necessary condition for stability, which is maintained within a set of values of parameters where the system is unstable (Table 1).

In the DR-S model any small perturbation in the system can change the dynamical behavior. If the DR-S system is subject to perturbations from neighboring faults, the seismic fault enters in a limit cycle, but it does not remain long there due to intervening stress perturbations (Dragoni and Santini, 2010).

3.3 The system under forcing conditions

This section aims to numerically describe the oscillatory behavior within and outside the range proposed for the SSO region Eq. (23), under forcing and nonforced conditions. We want to prove numerically that the proposed upper limit determines the changes in oscillatory behavior, below and above this. For more theoretical background into the theory of periodically forced systems near a point of Hopf bifurcation, see Zhang and Golubitsky (2011) and references therein.

We are interested in the oscillatory behavior when the values of parameters Π are nearest to the Hopf bifurcation. We numerically explored the effects of an external, deterministic and periodic force $\tau(t)$ acting on the system Eq. (5), for $\Pi = (0.25, 0.8, 0.8)$, $\alpha = (1.6, 0.2, 0.1)$, and $\mu = 3$. Such effects are illustrated by varying the angular frequency ω from $\tau(t) = \sin \omega t$. This numerical analysis is helpful for visualizing patterns in the dynamic of the system, especially those related to oscillatory behavior, such as limit cycles and periodic orbits.

Figure 6 shows numerical results of typical oscillations projected onto the plane (u, v) and time series generated by Eq. (5). The system Eq. (5) presents different behaviors when the parameter ω takes values in the interval [0.1,2]. For example when $\omega \in [0.1, 0.8]$, a type of complex behavior for low frequencies is observed (Fig. 6a). Figure 6b shows that for values of $\omega \in [0.8, 1.3]$, periodic orbits of period two are found. For angular frequencies $\omega > 1.3$ the flow of the system converges to a limit cycle, as shown in Fig. 6c. Conversely, Fig. 6d to f describe the time series of u when ω is 0.1, 1.2 and 2, respectively. The motion is periodical, this behavior emphasizes the periodic motion of the DR-S. The time series for low frequencies ($\omega < 0.8$) are more complex than the other cases.

3.3.1 Bifurcation diagram for unperturbed system

Qualitative changes in the dynamic of the system are better understood through bifurcation analysis, such as the case when a control parameter is varied and the bifurcations show the transitions or instabilities of the system. The unperturbed system is considered when $\tau(t) = \sin(\omega t) = 0$, i.e., $\omega = 0$. In order to show that the behavior of the unperturbed system displays SSO, the control parameter $\gamma = \sqrt{(k/M)}(L/v_0)$ is varied, which in turn is related to frequency of oscillation of the slider block and to the characteristic length of displacement L. Numerical results are for fixed $\xi = 0.8$, and the value for $\varepsilon = 0.25$ that holds the necessary condition Eq. (13).

Under the necessary condition Eq. (13), the system without external perturbations oscillates, and multi-periodic orbits are created over an approximate range of values $\gamma \in [0.6, 1]$. Eventually, the flow of the system converges to a limit cycle as is depicted in Figs. 7 and 8. This oscillatory behavior is observed when Π is nearest to the Hopf bifurcation in absence of external forces. The range of $u_{\text{lmax}}(t)$ decreases when γ increases.

3.3.2 Bifurcation diagram for perturbed system

According to previous outcomes, we considered the forced system $\tau(t) = \sin \omega t$ centered at $\omega = \{0.1, 1.2\}$, for fixed $\xi = 0.8$, and two values of ε. Two values for $\varepsilon = \{0.25, 1\}$ are explored. The first value holds the necessary condition and the second one does not. The bifurcation parameter is γ. We named case one of the analysis of bifurcation with fixed $\varepsilon = 0.25$, and the second case for $\varepsilon = 1$; for both cases $\xi = 0.8$ is fixed.

The bifurcation diagram for case one is displayed in Fig. 9, and it shows the qualitative behavior of system relative to the variable of position u and oscillation frequency γ. Figure 9 displays γ versus its local maximum of time series $u_{\text{lmax}}(t)$. Figure 9a for $\omega = 0.1$ shows that the most orbits are weakly attractive until approximate values of $\gamma > 0.9$ when limit cycles are observed.

Conversely, Fig. 9b for $\omega = 1.2$ shows limit cycles, which are observed approximately when $\gamma \in [0.55, 0.66]$, $\gamma > 1.17$, and $\gamma = .765$; whereas there are two points of bifurcation from orbits of period one to orbits of period two at $\gamma = 0.66$ and $\gamma = 0.765$. The orbits of period two have the form of Fig. 6b, and the limit cycles take the form as in Fig. 6c. The orbits are strongly attractive, which suggests that they could be stable at least during a short period. According to the necessary condition for stability, the behavior of $u_{\text{lmax}}(t)$ relative to γ decreases for both $\omega = 0.1$ and $\omega = 1.2$ because after γ reaching the values 0.9 and 1.17, respectively, the system falls into the limit cycle, in such a way that when γ increases, the range of values for $u_{\text{lmax}}(t)$ decrease. The type of behavior displayed in Fig. 9 is expected when $\varepsilon < \xi \psi$.

Table 1. Relationship between parameters Π on the oscillatory range for Fig. 4a and b ε_{HB} is the value of the Hopf bifurcation; $(\pm\lambda_{1,2})_{HB}$ is the eigenvalues on the imaginary axis; $\varepsilon_{D=0}$ is the value when the discriminant of the characteristic polynomial is equal to zero, i.e., the upper limit of OR; SSO is the interval of self-sustained oscillations; and $r'(\Pi_0)$ is the cross-velocity of eigenvalues.

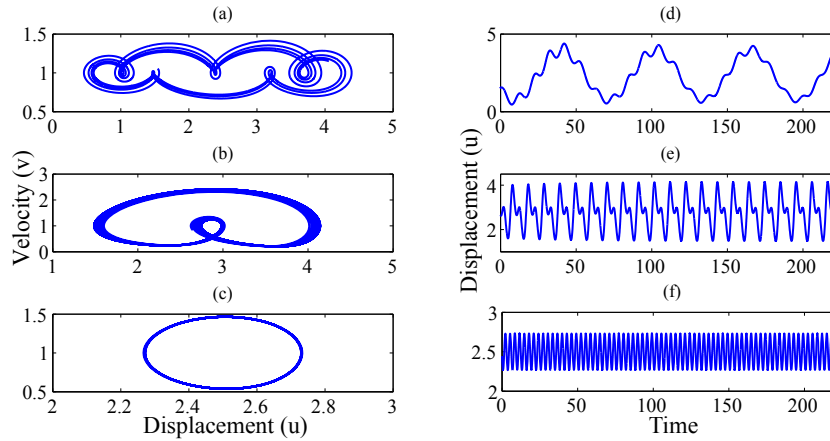| γ	ξ	ε_{HB}	$\pm(\lambda_{1,2})_{HB}$	$\varepsilon_{D=0}$	SSO$\in (\varepsilon_{HB}, \xi_0\psi_0)$	$r'_\varepsilon(\Pi_0)$
0.8	0.4	0.1981	0.5030i	2.081779482130000	(0.1981,0.3562)	0.3042
	0.8	0.2499	0.6083i	3.704570372000000	(0.2499,0.7123)	0.2058
	1.0	0.2534	0.6385i	4.507300000000000	(0.2534,0.8904)	0.1749
10	0.4	0.3981	0.6313i	1.668570861615000	(0.3981,0.3997)	0.4981
	0.8	0.7931	0.8911i	2.601243068598171	(0.7931,0.7994)	0.4963
	1.0	0.9894	0.9954i	3.018387963893687	(0.9894,0.9993)	0.4953

Figure 6. Projection of the attractor onto the plane (u, v) and time series of the perturbed system 5. Panels **(a)**, **(b)**, and **(c)** show the projection onto the plane for $\omega = 0.1, 1.2,$ and 2, respectively. Panels **(d)**, **(e)**, and **(f)** display their respective time series for u.

The region of SSO could be numerically explained by this analysis; if the system is perturbed slightly by external forces $\tau(t)$, it always returns to the standard cycle.

The bifurcation diagram for case two is displayed in the Fig. 10a for $\omega = 1.2$. The necessary condition Eq. (13) fails; and the dynamic of the system shows three types of behavior: behavior Type I (Fig. 10b) is observed approximately at $\gamma \in (0.6, 1.55)$. Type I shows periodic orbits of period one and two that appear to be alternating, and bifurcations from orbits of period one to period two occur, then the system reaches a limit cycle at $\gamma = 1.55$ but now with Type II behavior for approximate values of $\gamma \in (1.55, 3.5)$. In Type II, $u_{lmax}(t)$ increases while maintaining the limit cycle until behavior Type III is observed approximately for $\gamma \in (3.5, 5.5)$, which displays periodic orbits with different period. The behavior displayed in Fig. 10 corresponds to an unstable and oscillatory region outside of the SSO.

3.4 Type of Hopf bifurcation

In terms of the flow in phase space, a supercritical Hopf bifurcation occurs when a stable spiral changes into an unstable spiral surrounded by nearly elliptical limit cycle (Strogatz, 1994). A subcritical Hopf bifurcation occurs when a small perturbation can lead to either decaying oscillations due to a stable equilibrium or a jump to large sustained oscillations in the system due to an unstable limit cycle. For the analysis of the bifurcation type, the main challenge is the numerical stiffness, due to the nonlinear logarithmic term.

The set of parameters Π does not cross the Hopf bifurcation if $\gamma > \gamma_{HB}$. Small disturbances decay after ringing for a while and a stable spiral is observed. The block and the driver plate are moving at constant rate $v = 1$, and the relative position is η. Conversely, for $\gamma < \gamma_{HB}$, the parameter values cross the Hopf bifurcation. The equilibrium state loses stability and an unstable spiral is observed. This type of bifurcation is expected for smooth, noncatastrophic changes (see Supplement). The slow earthquakes are almost imperceptible because the displacement rate is very low compared to ordinary earthquakes and they are generated for parameter values around the critical value of nucleation. Hopf bifurcation is supercritical within the proposed limits for unforced system. To find chaotic behavior or strange attractors with the nonforced system it is necessary to vary epsilon very far (Erickson et al., 2008) from the value of the Hopf bifurcation that we are analyzing.

However, Kostić et al. (2013) have found chaotic behavior for small values of Π by introducing a time delay in the
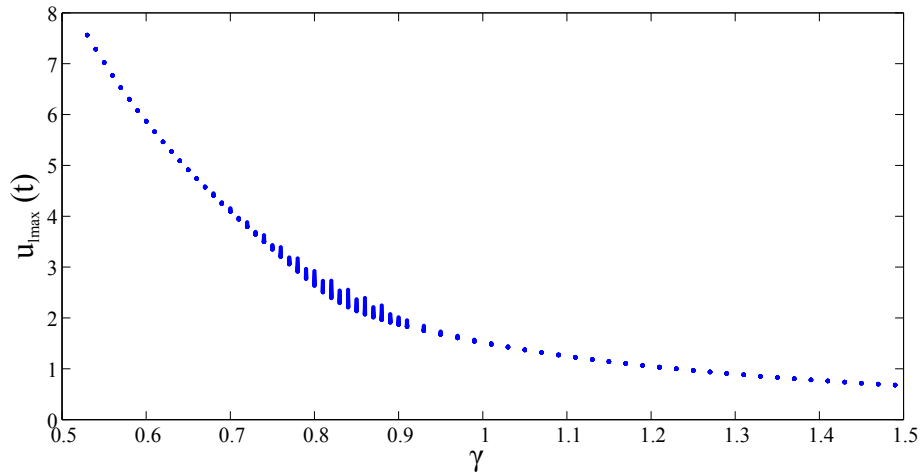
Figure 7. Bifurcation diagram for an unperturbed system $\tau(t) = 0$, bifurcation parameter γ versus local maximum of time series $u_{\mathrm{lmax}}(t)$, and $\Pi = (0.25, 0.8, \gamma)$.
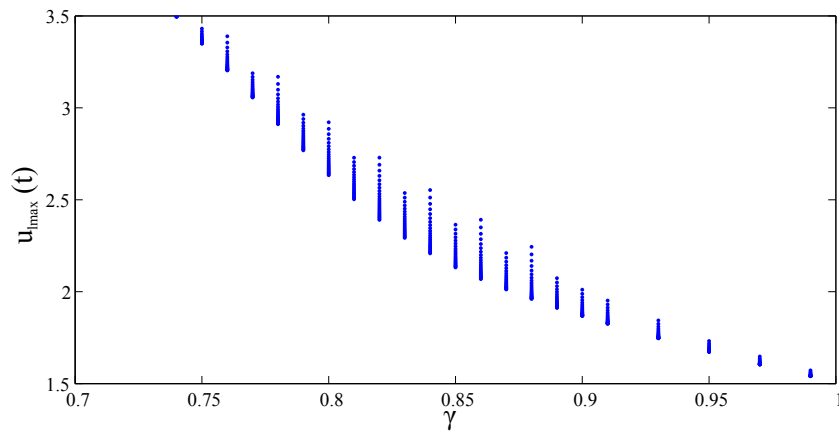

Figure 8. An enlarged view of Fig. 7.

friction term. They have found two types of Hopf bifurcation depending on the variation of the time delay. Similarly, by introducing the external force $\tau(t)$ a subcritical Hopf bifurcation could be given for some critical $\tau(t)$ and slight variation of the ε and ξ parameters. Disturbances do not allow the system to remain at an equilibrium point, resulting in continuous oscillations or chaos. For the case when the set of parameters Π crosses the Hopf bifurcation, continuous oscillations were found in both displacement and velocity only by varying the bifurcation parameter (see Supplement). Determining critical values of Π and $\tau(t)$ requires more concrete study.

4 Discussion and conclusions

We have analyzed the DR-S model, which describes the kinetic mechanism during an earthquake. The system displays richness in their oscillatory dynamic behavior: from attracting cycles of one and two periods to a limit cycle and multi-

periodic orbits, depending on the parameter values in the necessary condition for stability Eq. (13). The necessary condition is maintained even for a set of parameters within the frictionally unstable region. This behavior was studied by bifurcation diagrams through the Hopf bifurcation mechanism.

The complex oscillatory behavior discussed in this paper is determined by the variation of parameter γ, fixed values ε and ξ, and the necessary condition for stability Eq. (13). The necessary condition depends on the parameter γ, and this depends on the characteristic length L, suggesting that the complex oscillatory behavior should be observed for a range of values for the parameter γ. The unperturbed and perturbed cases have shown how the system describes behavior as it is found in systems with SSO; this is in the case when the necessary condition Eq. (13) is maintained (Figs. 7 and 9). There are self-oscillations that create multi-periodic orbits but eventually converge to a limit cycle and the range of $u_{\mathrm{lmax}}(t)$ decreases when γ increases.
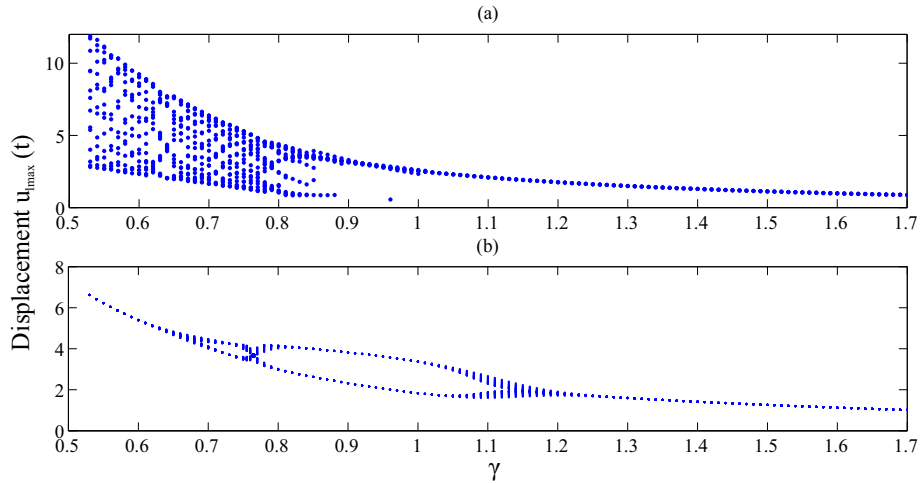
Figure 9. Bifurcation diagram γ versus local maximum from the time series $u_{\mathrm{lmax}}(t)$ $\mathbf{\Pi} = (0.25, 0.8, \gamma)$, $\mu = 3$, $\boldsymbol{\alpha} = (1.6, 0.2, 0.1)$, subdamped system. In panel **(a)** $\omega = 0.1$, and in **(b)** $\omega = 1.2$.
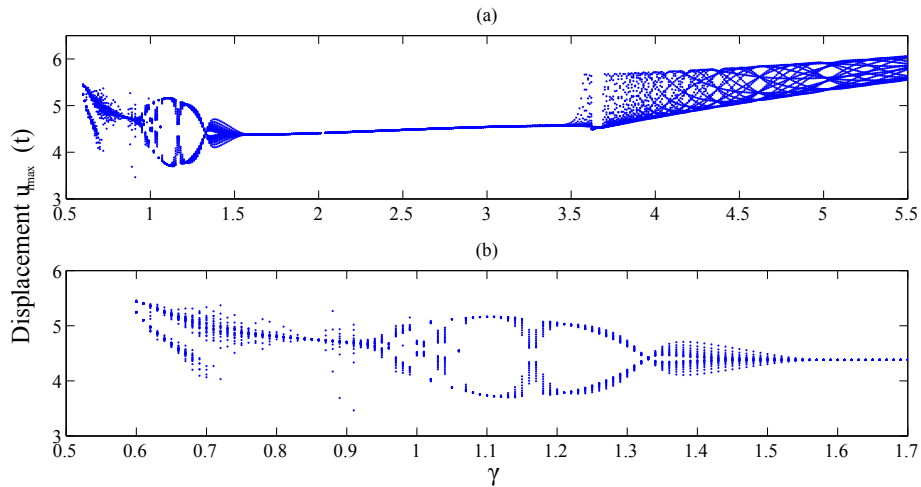

Figure 10. Bifurcation diagram γ versus local maximum from time series $u_{\mathrm{lmax}}(t)$, $\omega = 1.2$, $\mathbf{\Pi} = (1, 0.8, \gamma)$ $\mu = 3$, $\boldsymbol{\alpha} = (1.6, 0.2, 0.1)$, sub-damped system. **(a)** There are three types of behavior: Type I, II, and III. **(b)** Enlarged view of Type I.

The γ parameter seems to be relevant, and consequently the characteristic length L. Lapusta et al. (2000), Lapusta and Rice (2003), and Abe and Kato (2013) derived some conclusions concerned with L from laboratory experiments and numerical simulations. They associated L with the size of small earthquakes, with frequency, and with SSO. If L decreases then the block is frictionally less stable, i.e., there are more frequent displacements; moreover, they found that under a range of parameter values the oscillations can change from periodic to aperiodic and vice versa, but the border of the transition was not defined.

Under the assumption $B > A > 0 \rightarrow \varepsilon > 0$ and Eq. (20), Hopf bifurcation occurs for any $\gamma \geq 0.5$ within the standard $0.4 < \xi_0 < 1$; moreover, $\varepsilon_{\mathrm{HB}} \rightarrow \xi_0$ when γ increases in such way that for any $\gamma \geq 10$ the values of $\varepsilon_{\mathrm{HB}}$ are equal. For these values, ε is bounded in $0 < \varepsilon_{\mathrm{HB}} < 1$.

This would have some implications related to the slow-earthquake nucleation. For the SSO region, for $0.5 < \gamma \leq 10$, the oscillation frequency and fluid are approximately determinant for the systems that have unstable oscillations. For small values of γ there are more transitions in the dynamical oscillatory behavior, when the necessary condition Eq. (13) holds and does not it as it is shown in Figs. 7, 9, and 10. On the other hand, for $\gamma \geq 10$ there are less transitions, and neither the fluid nor frictional coefficients of Stribeck in the medium affect the oscillatory behavior ($\phi/\gamma^2 \rightarrow 0 \rightarrow \psi \rightarrow 1$).

This general behavior for small γ seems to be independent of the angular frequency, ω, of the external force because even the unperturbed system displays this behavior. The function of the ω variation is the generation of the dominant type of orbits (one, two, or more periods) and its fre-

quency of transition, which is bigger when the necessary condition fails. The complex oscillatory behavior is dependent on small γ values and of the necessary condition for stability Eq. (13) that involves fluids from Stribeck's effect.

The relevance of γ seems to be associated with the presence of fluid. Erickson et al. (2008) determined that the stationary solution $\boldsymbol{x}^* = (0, 0, 1)$ is independent of seismic parameters, and the relative position of the block and the plate will not depend on the frictional coefficients or seismic parameters; the system would be under the limit of the unstable regime where the big earthquakes are nucleated. At this solution the block and the plate have the same velocity and there is no contact with asperities, and hence there is no displacement between the plate and the slider block.

Complementarily, we found if Stribeck's effect is added to the Madariaga model then the stationary solution $\boldsymbol{x}^* = (0, \eta, 1)$ has the displacement or relative position as a function of seismic parameter γ. The parameter γ is associated with the oscillation frequency of the block as well as the frictional constants related to fluid through ψ in the necessary condition Eq. (13).

The relative position u is not necessarily zero, although the relative displacement is. The role of frequency oscillations and fluid is decisive for dissipation and consequently it is also for the block position. If γ is large enough then $\boldsymbol{x}^* \to (0, 0, 1)$, i.e., if γ or kL increases, then $u^* \to 0$. The last statement could be interpreted as k increases making the system stiffer or L increases making the stress drop slower under some conditions.

The stability analysis of $\boldsymbol{x}^*$ was through eigenvalues of Eq. (8). If the real part is negative for all eigenvalues then the stationary solution is a sink and the system is in the stable regime, the medium properties break any nucleation or propagation of earthquakes. Scholz (1998) determined a critical value for frictional stability or instability under an elastic medium, with an oscillator coupled to the Dieterich friction law,

$$\overline{\sigma}_c = \frac{-kL}{a - b}, \tag{24}$$

that depends on the rocks properties, point nucleation, and frictional parameters $a - b$, k, yL. The critical value $\overline{\sigma}_c$ corresponds to the normal effective stress. When any $\overline{\sigma}$ holds $\overline{\sigma} \geq \overline{\sigma}_c$, then there are changes in the frictional properties, such changes unchained earthquakes. This phenomena is named frictional instability. Scholz (1998) reported that the SSOs are in the stable regime, below the critical value of nucleation Eq. (24) (Fig. 1). In a complementary way this investigation reveals that the critical value Eq. (24) of Scholz (1998) have got to the upper limit of SSO in the unstable region, and it is related to the upper limit of SSO in the frictionally unstable region regardless of the Stribeck effect.

The relation between the SSO Eqs. (23) and (24) comes from the definition of $\boldsymbol{\Pi} = (\varepsilon, \xi, \gamma)$ and the statement $(A - B) = \sigma(a - b)$ (Daub and Carlson, 2008) as fol-

lows. From Eq. (24) $\overline{\sigma}_c(b - a) = kL \to (B - A) = kL \to (B - A)/A = kL/A \to \varepsilon = \xi$; conversely $\varepsilon = \xi \psi \to \overline{\sigma}_c(b - a)/A < kL\psi/A \to \overline{\sigma}_c = -kL\psi/(a - b)$. A corrected value for SSO is as follows:

$$1 < \overline{\sigma}_c^* \equiv \frac{-kL\psi}{(a - b)} \equiv \overline{\sigma}_c \psi, \tag{25}$$

which combines frictional parameters of Dieterich–Ruina friction law and Stribeck's effect. Equations (13) and (25) are equivalent, if $\gamma > 10$, $\psi \to 1$ and $\overline{\sigma}_c^* \to \overline{\sigma}_c$.

The upper limit of SSO behavior is a function of seismic parameters and frictional coefficients concerned with fluids, although this was established for the base of seismogenic layer, it is likely that it could be applied to the shallow transition zone in addition to the parameters and constants related to the slip-hardening (Ikari et al., 2013). The fluid presence involves the frequency of oscillation of the block as a very important element to dissipation and consequently with the stationary solution (equilibrium point of the system) as well as in the upper limit proposed for slow-earthquake zones. The characteristic length L has primary relevance for the results of this research.

Although this investigation is more related to the proposal of a formal pattern in the study of slow slip earthquakes (SSEs), and with a first approximation of the upper limit of the transition zone, this is considered as a preliminary study in order to be applied to the real seismogenic regions. However, the parameters considered for slow earthquakes are still being studied through observations, experiments, and by means of simulations, but there is still not something precise.

The study of SSEs in Cascadia (Watkins et al., 2015) indicates a possible link between the observational and experimental data, with the parameters involved in the most of models of earthquake's physic coupled to the Dieterich–Ruina's friction law. The slip amount of SSEs is on centimeter scale but the average slip amount of smaller events are unknown. The effective normal stress in the range of 3–9 MPa produces a fault slip consistent with some observed SSEs, and $B - A$ is in the range (0.0015 to 0.003) of the slow slip section. At the top of the slow slip section $B - A$ is 0.003 and 0.001 at the base, $A \approx 0.02$, L is in the range 1–50 µm (real L is unknown), and the rate of convergence (10–50 mm yr^{-1}) represents the range of convergence rates of subduction zones where SSEs are observed with GPS. These parameters could vary depending on the region in which SSEs occur. Further, the critical value $K_c = (A - B)\sigma/L$ depends on L; viscosity $= 0.1$ (nondimensional) has been used in earthquake models (Carlson et al., 1994), but the estimation of the real viscosity depends on the region.

The proposed upper limit for the SSE zone includes the fluids and oscillation frequency (and consequently L), through ψ. They might be introduced into the simulations and experiments in order to see what the implications are for the recurrence times, duration, and velocity of SSEs in real seismogenic regions. A final step would be using scal-

ing laws for SSEs to determine whether the real values of parameters included either experimental and/or simulation data, such as the stiffness K_c and viscosity, take into account the specific characteristics of the fault.

The Supplement related to this article is available online at https://doi.org/10.5194/npg-24-419-2017-supplement.

References

Abe, Y. and Kato, N.: Complex Earthquake Cycle Simulations Using a Two-Degree-of-Freedom Spring-Block Model with a Rate- and State-Friction Law, Pure Appl. Geophys., 170, 745–765, 2013.

Abe, Y. and Kato, N.: Intermittency of earthquake cycles in a model of a three-degree-of-freedom spring-block system, Nonlin. Processes Geophys., 21, 841–853, https://doi.org/10.5194/npg-21-841-2014, 2014.

Alvarez-Ramírez, J., Garrido, R., and Femat, R.: Control of systems with friction, Phys. Rev. E, 51, 6235, https://doi.org/10.1103/PhysRevE.51.6235, 1995.

Amendola, A. and Dragoni, M.: Dynamics of a two-fault system with viscoelastic coupling, Nonlin. Processes Geophys., 20, 1-10, https://doi.org/10.5194/npg-20-1-2013, 2013.

Andersson, S., Söderberg, A., and Björklund, S.: Friction models for sliding dry, boundary and mixed lubricated contacts, Tribol. Int., 40, 580–587, 2007.

Audet, P. and Bürgmann, R.: Dominant role of tectonic inheritance in supercontinent cycles, Nat. Geosci., 4, 184–187, 2011.

Baca, D.: Análisis paramétrico de la bifurcación de Hopf en sistemas tipo Lorentz, Tesis: Universidad de Sonora, Hermosillo, México, 2007.

Batista, A. A. and Carlson, J. M.: Bifurcations from steady sliding to stick slip in boundary lubrication, Phys. Rev. E, 57, 4986–4996, 1998.

Beroza, G. C. and Ide, S.: Deep tremors and slow quakes, Science, 324, 1025–1026, https://doi.org/10.1126/science.1171231, 2009.

Brown, K. M., Tryon, M. D., DeShon, H. R., Dorman, L. M., and Schwartz, S. Y.: Correlated transient fluid pulsing and seismic tremor in the Costa Rica subduction zone, Earth Planet. Sc. Lett., 238, 189–203, 2005.

Bürgmann, R.: Earth science: Warning signs of the Iquique earthquake, Nature, 512, 258–259, 2014.

Campos-Cantón, E., Barajas-Ramírez, J. G., Solís-Perales, G., and Femat, R.: Multiscroll attractors by switching systems, Chaos, 20, 013116, https://doi.org/10.1063/1.3314278, 2010.

Carlson, J. M., Langer, J. S., and Shaw, B. E.: Dynamics of earthquake faults, Rev. Mod. Phys., 66, 657–670, 1994.

Carlson, J. M. and Batista, A. A.: Constitutive relation for the friction between lubricated surfaces, Phys. Rev. E, 53, 4153–4165, 1996.

Castellanos-Rodríguez, V. and Femat, R.: A model for earthquakes based on friction effects: Oscillatory aperiodic behavior, Analysis and Control of Chaotic Systems, 3, 115–120, 2012.

Chelidze, T., Matcharashvili, T., Gogiashvili, J., Lursmanashvili, O., and Devidze, M.: Phase synchronization of slip in laboratory slider system, Nonlin. Processes Geophys., 12, 163–170, https://doi.org/10.5194/npg-12-163-2005, 2005.

Daub, E. G. and Carlson, J. M.: A constitutive model for fault gouge deformation in dynamic rupture simulations, J. Geophys. Res.-Sol. Ea., 113, B12, https://doi.org/10.1029/2007JB005377, 2008.

Davis, E., Heesemann, M., and Wang, K.: Evidence for episodic aseismic slip across the subduction seismogenic zone of Costa Rica: CORK borehole pressure observations at the subduction prism toe, Earth Planet. Sc. Lett., 306, 299–305, https://doi.org/10.1016/j.epsl.2011.04.017, 2011.

De sousa Vieira, M.: Chaos in a simple spring-block system, Phys. Lett. A, 198, 407–414, 1995.

Dieterich, J. H.: Modeling of Rock Friction, 1, Experimental Results and Constitutive Equations, J. Geophys. Res., 84, 2161–2168, 1979.

Dieterich, J. H. and Kilgore, B. D.: Direct observation of frictional contacts: New insights for state-dependent properties, Pure Appl. Geophys., 143, 283–302, 1994.

Di Toro, G., Han, R., Hirose, T., De Paola, N., Nielsen, S., Mizoguchi, K., Ferri, F., Cocco, M., and Shimamoto, T.: Fault lubrication during earthquakes, Nature, 471, 494–498, 2011.

Dragert, H., Wang, K., and James, T. S.: A Silent Slip Event on the Deeper Cascadia Subduction Interface, Science, 292, 1525–1528, 2001.

Dragoni, M. and Piombo, A.: Dynamics of a seismogenic fault subject to variable strain rate, Nonlin. Processes Geophys., 18, 431–439, https://doi.org/10.5194/npg-18-431-2011, 2011.

Dragoni, M. and Santini, S.: Simulation of the long-term behaviour of a fault with two asperities, Nonlin. Processes Geophys., 17, 777–784, https://doi.org/10.5194/npg-17-777-2010, 2010.

Erickson, B., Birnir, B., and Lavallée, D.: A model for aperiodicity in earthquakes, Nonlin. Processes Geophys., 15, 1–12, https://doi.org/10.5194/npg-15-1-2008, 2008.

Faulkner, D. R., Jackson, C. A. L., Lunn, R. J., Schlische, R. W., Shipton, Z. K., Wibberley, C. A. J., and Withjack, M. O.: A review of recent developments concerning the structure, mechanics and fluid flow properties of fault zones, J. Struct. Geol., 32, 1557–1575, 2010.

Gee, M. L., McGuiggan, P. M., Israelachvili, J. N., and Homola, A. M.:Liquid to solidlike transitions of molecularly thin films under shear, J. Chem. Phys., 93, 1895–1906, 1990.

Gu, J., Rice, J. R., Ruina, A., and Tse, S.: Slip motion and stability of a single degree of freedom elastic system with rate and state dependent friction, J. Mech. Phys. Solids, 32, 167–196, 1984.

Guckenheimer, J. and Holmes, P.: Nonlinear oscillations, dynamical systems, and bifurcations of vector fields, Springer Verlag, New York, 42, 1983.

Ide, S., Beroza, G. C., Shelly, D. R., and Uchide, T.: A scaling law for slow earthquakes, Nature, 447, 76–79, https://doi.org/10.1038/nature05780, 2007.

Ikari, M. J., Marone, C., Saffer, D. M., and Kopf, A. J.: Slip weakening as a mechanism for slow earhtquakes, Nat. Geosci., 6, 468–472, 2013.

Jacobson, B.: The Stribeck memorial lecture, Tribol. Int., 36, 781–789, 2003.

Jolivet, R., Lasserre, C., Doin, M., Peltzer, G., Avouac, J., Sun, J., and Dailu, R.: Spatio-temporal evolution of aseismic slip along the Haiyuan fault, China: Implications for fault frictional properties, Earth Planet. Sc. Lett., 377, 23–33, https://doi.org/10.1016/j.epsl.2013.07.020, 2013.

Kengne, J., Kenmogne, F., and Kamdoum Tamba, V.: Experiment on Bifurcation and Chaos in Coupled Anisochronous Self-Excited Systems: Case of Two Coupled van der Pol-Duffing Oscillators, Journal of Nonlinear Dynamics, 2014, 815783, https://doi.org/10.1155/2014/815783, 2014.

Khalil, M.: Nonlinear Systems, Second edition, Prentice-Hall, 1996.

Kostić, S., Franović, I., and Todorović, K.: Friction memory effect in complex dynamics of earthquake model, Nonlinear Dynam., 73, 1933–1943, https://doi.org/10.1007/s11071-013-0914-8, 2013.

Lapusta, N. and Rice, J.: Nucleation and seismic early propagation of small and large events in a crustal earthquakes model, J. Geophys. Res., 108, B4, https://doi.org/10.1029/2001JB000793, 2003.

Lapusta, N., Rice, J., Ben-Zion, Y., and Zheng, J.: Elastodynamic analysis for slow tectonic loading with spontaneous rupture episodes on faults with rate-and state-dependent friction, J. Geophys. Res., 105, 23765–23789, 2000.

Levin, V. W.: Non-linear oscillating structures in the earthquake and seaquake dynamics, Chaos, 6, 405–413, 1996.

Maloney, C. E. and Robbins, M. O.: Shear faults in a model brittle solid, Chaos, 17, 041105, https://doi.org/10.1063/1.2786010, 2007.

Marone, C., Scuderi, M., Leeman, J., Saffer, D., Collettini, C., and Johnson, P.: Slow earthquakes and the mechanics of slow frictionalstick-slip, Gephysical Research Abstracts, 17, EGU2015-9533, EGU General Assembly, 2015.

Meng, X. Y. and Huo, H. F.: Bifurcation Analysis of a Lotka-Volterra Mutualistic System with Multiple Delays, Abstract and Applied Analysis, 2014, 958140, 2014.

Nishimura, T.: Short-term slow slip events along the Ryukyu Trench, southwestern Japan, observed by continuous GNSS, Prog. Earth Planet. Sci., 1, 22, https://doi.org/10.1186/s40645-014-0022-5, 2014.

Peng, Z. and Gomberg, J.: An integrated perspective of the continuum between earthquakes and slow-slip phenomena, Nat. Geosci., 3, 599–607, 2010.

Perko, M. J., Jarnvig, I. L., Hojgaard-Rasmussen, N., Eliasen, K., and Arendrup, H.: Electric impedance for evaluation of body fluid balance in cardiac surgical patients, J. Cardiothor. Vasc. An., 15, 44–48, 2001.

Reiter, G., Demirel, A. M., and Granick, S.: From Static to Kinetic Friction in Confined Liquid Films, Science, 263, 1741–1744, 1994.

Rivet, D., Campillo, M., Shapiro, N. M., Cruz-Atienza, V., Radiguet, M., Cotte, N., and Kostoglodov, V.: Seismic evidence of nonlinear crustal deformation during a large slow slip event in Mexico, Geophys. Res. Lett., 38, L08308, https://doi.org/10.1029/2011GL047151, 2011.

Ruina, A.: Slip instability and state variable friction laws, J. Geophys. Res.-Sol. Ea., 88, 10359–10370, 1983.

Saffer, D. and Wallace, L. M.: The frictional, hydrologic, metamorphic and thermal habitat of shallow slow earthquakes, Nat. Geosci. 8, 594–600, https://doi.org/10.1038/ngeo2490, 2015.

Scholz, C. H.: Earthquakes and friction laws, Nature, 391, 37–42, 1998.

Scuderi, M., Marone, C., Tinti, E., Scognamiglio, L., Leeman, J., Saffer, D., Di Stefano, G., and Collettini, C.: Seismic velocity changes across the transition from slow-to fast-frictional sliding in earthquake-like laboratory experiments, AGU Chapman Conference in the Slow Slip Phenomena, Ixtapa, Guerrero, Mexico, 21–26 February, 2016.

Shkoller, S. and Minster, J.-B.: Reduction of Dietrich-Ruina attractors to unimodal maps, Nonlin. Processes Geophys., 4, 63–69, https://doi.org/10.5194/npg-4-63-1997, 1997.

Strogatz, S. H: Nonlinear Dynamics and Chaos: with application to physics, biology, chemistry, and engineering, Perseus Book Publishing, 1994.

Thomas, A., Beroza, G., and Shelly, D.: Constraints on the source parameters of low-frequency earthquakes on the San Andreas Fault, Geophys. Res. Lett., 43, 1464–1471, https://doi.org/10.1002/2015GL067173, 2016.

Valée, M.; Nocquet, J., Battaglia, J., Font, Y., Segovia, M., Régnier, M., Mothes, P., Jarrin, P., Cisneros, D., Vaca, S., Yepes, H., Martin, X., Béthoux, N., and Chlieh, N.: Intense interface seismicity triggered by a shallow slow slip event in the Central Ecuador subduction zone, J. Geophys. Res., 118, 2965–2981, 2013.

Vergnolle, M., Walpersdorf, A., Kostoglodov, V., Tregoning, P., Santiago, J. A., Cotte, N., and Franco, S. I.: Slow slip events in Mexico revised from the processing of 11 year GPS observations, J. Geophys. Res., 115, B8, https://doi.org/10.1029/2009JB006852, 2010.

Wallace, L. M., Webb, S. C., Ito, Y., Mochizuki, K., Hino, R., Henrys, S., Schwartz, S., and Sheehan, A.: Slow slip near the trench at the Hikurangi subduction zone, New Zealand, Science, 352, 701–704, https://doi.org/10.1126/science.aaf2349, 2016.

Wang, H., Yu, Y., and Wen, G.: Dynamical Analysis of the Lorenz-84 Atmospheric Circulation Model, J. Appl. Math., 2014, 296279, https://doi.org/10.1155/2014/296279, 2014.

Watkins, W. D., Colella, H. V., Brudzinski, M. R., Richards-Dinger, K. B., and Dieterich, J. H.: The role of effective normal stress, frictional properties, and convergence rates in characteristics of simulated slow slip events, Geophys. Res. Lett., 42, 1061–1067, https://doi.org/10.1002/2014GL062794.

Wech, A. G. and Creager, K. C.: Cascadia tremor polarization evidence for plate interface slip, Geophys. Res. Lett., 34, https://doi.org/10.1029/2007GL031167, 2007.

Yamashita, Y., Yakiwara, H., Asano, Y., Shimizu, H., Uchida, K., Hirano, S., Umakoshi, K., Miyamachi, H., Nakamoto, M., Fukui, M., Kamizono, M., Kanehara, H., Yamada, H., Shinohara, M., and Obara, K.: Migrating tremor off southern Kyushu as evidence for slow slip of a shallow subduction interface, Science, 348, 676–679, https://doi.org/10.1126/science.aaa4242, 2015.

Yoshizawa, H. and Israelachvili, J.: Fundamental mechanisms of interfacial friction. 2. Stick-slip friction of spherical and chain molecules, J. Phys. Chem., 97, 11300–11313, 1993.

Zhang, Y. and Martin Golubitsky, M.: Periodically Forced Hopf Bifurcation, SIAM Journal of Applied Dynamical Systems, 10, 1272–1306, 2011.